J Mater Sci (2011) 46:6384–6389
DOI 10.1007/s10853-011-5586-5

Improved mechanical properties in Ti-bearing martensitic steel by precipitation and grain refinement

L. Xu · J. Shi · W. Q. Cao · M. Q. Wang · W. J. Hui · H. Dong

Received: 21 March 2011 / Accepted: 22 April 2011 / Published online: 4 May 2011

Abstract The yield strength and impact energy properties for martensitic steel fabricated by vacuum induction melting are investigated. It is found that the addition of Ti can improve the yield strength property of the martensitic steel after reheat quenching process, which can be attributed to increase in precipitation hardening from formation of TiC precipitates in the martensitic matrix and a superfine sized (~8 μm) grains in the martensitic structure. Moreover, the yield strength can be further enhanced by tempering and reheat quenching process, which can be ascribed to a large amount of freshly nano-sized (1–10 nm) precipitates in the final martensitic structure for martensitic steel-containing Ti. The experimental and theoretical results on the contribution of TiC precipitates to hardening of the martensitic steel are in excellent agreement. In addition, the impact toughness also has been improved along with yield strength followed by the heat treatment, which can be attributed to the high ratio of high-angle grain boundaries after tempering and reheat quenching process.

Introduction

Martensitic steels are very important metallic materials. Their outstanding properties are high strength [1], excellent ductility [2], and good weldability [3], which make them have been used in a variety of applications, including pipelines [4], gas turbines [5], compressor wheels, blades [6], bolts, and sheet structures [7]. The strength of conventional martensitic steel was mainly related to its carbon content [8, 9] and alloy content [10, 11]. However, it is well known that precipitation hardening [12] and grain refinement hardening [13] are also a promising approach to increase the strength of steels, but few study is carried out in the martensitic steels at present time. Therefore, further investigation is required to promote our understanding of these phenomena.

As a transition metal, titanium has numerous attractive properties, such as low density, good strength [14], which is also a strong carbide-forming element. It was expostulated that the titanium carbide precipitates can not only improve the strength by precipitation hardening but also refine the grain size by pinning of precipitation. Based on this idea, the martensitic steel-containing Ti to form precipitates was designed and fabricated by vacuum induction melting. The precipitation hardening and grain refinement caused by TiC precipitates and their effect on the yield strength and impact toughness of martensitic steel during different heat treatments are reported.

Experimental

Table 1 shows the chemical compositions of the designed steel used in this study. The steel was fabricated by vacuum induction melting. The ingots were homogenized at 1250 °C with 2 h, forged in between 1200 and 850 °C into a plate of 30 × 200 × 100 mm. The hot-rolling simulation was done using a pilot mill with a prepared slab of 30 mm in thickness. The basic thermomechanical pattern was shown in Fig. 1. The slab was soaked at 1250 °C for 2 h in a muffle furnace, and then hot rolled into strips of 7 mm in thickness through four passes. The plates were finally rolled at about 850 °C and water quenched to room

L. Xu (✉) · J. Shi · W. Q. Cao · M. Q. Wang · W. J. Hui · H. Dong
National Engineering Research Center of Advanced Steel Technology (NERCAST), Central Iron and Steel Research Institute (CISRI), Beijing 100081, People's Republic of China
e-mail: never_stop_exploring@live.cn

Table 1 Chemical compositions of steel used (mass%)

C	Mn	Ti	B	P	S	[N]
0.2	1.5	0.16	0.003	0.005	0.004	0.003

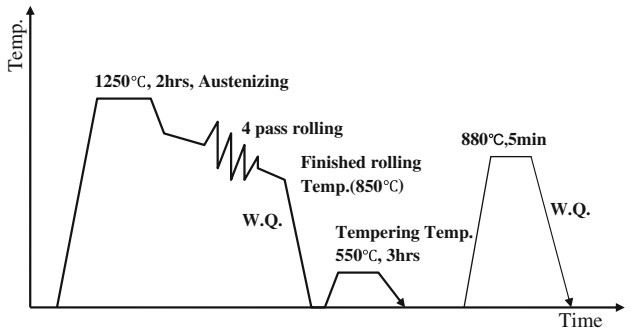

Fig. 1 The basic thermomechanical pattern for the samples

temperature after final deformation. Then, the as-quenched plate was soaked at 880 °C for 5 min in a muffle furnace and water quenched to room temperature. For comparison, the plate was soaked at 880 °C for 5 min in a muffle furnace and water quenched to room temperature to obtain the martensitic matrix after tempering at 550 °C for 3 h.

The microstructure was characterized by HITACHI H-800 type transmission electron microscopy (TEM). To reveal the prior austenite grains, the specimens were etched with a supersaturated picric acid aqueous solution after mechanical polishing. The prior austenite grain sizes in the experimental steel were determined by linear intercept measurements on optical micrographs. Thin-foil specimens for TEM observations were cut from the specimens and prepared by twin-jet electrolytic polishing using a solution of 10% perchloric acid and 90% ethanol at 243 K. The average diameter and size distribution of precipitates were analyzed and calculated by phase analysis method. Meanwhile, the phase structures of precipitates were identified by X-ray diffraction. EBSD orientation maps were observed using JEM-2100. The method of electrolytically extracted phase analysis was used to determine the structure, the wt%, and size distribution of precipitates. Tensile test was performed on the dog-bone-shaped specimens with gauge length of 25 mm and diameter of 5 mm at a strain rate of 10^{-3}/s in an Instron machine at room temperature. Charpy V-notch impact test was carried out at −40 °C using a cryo chamber on FIE 300J capacity charpy impact testing machine.

Results and discussion

Figure 2 exhibits the TEM images for as-quenched sample A, reheat quenching sample B, and tempering–reheat quenching sample C, respectively. The relative bulky precipitates can be observed in sample A (Fig. 2a), which is attributed to precipitate in austenite during the hot-rolling process. However, as the reheat quenching process is

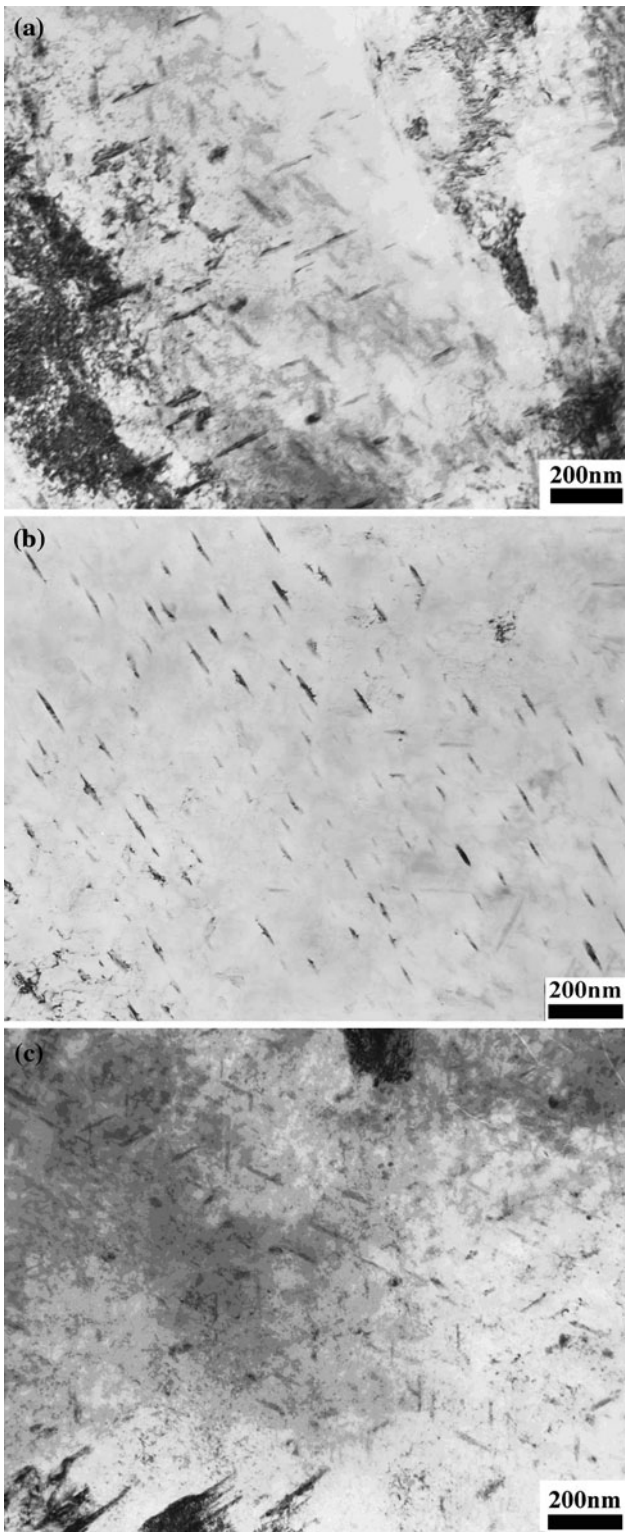

Fig. 2 TEM images for **a** sample A, **b** sample B, and **c** sample C

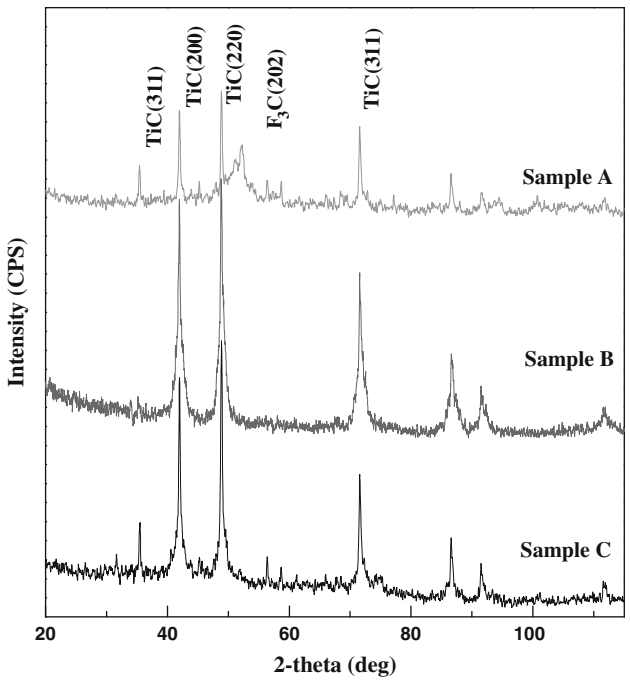

Fig. 3 The XRD patterns for the samples A–C

Table 2 The phase analysis results for the samples A–C (mass%)

Sample	A	B	C
Precipitation content of Ti	0.092	0.139	0.16
Precipitation content of C	0.023	0.035	0.04

introduced, the density of precipitates in reheat quenching sample B (Fig. 2b) becomes higher. As for the sample C (Fig. 2c), the size and density of precipitates change remarkably compared with sample A. The sample C has the maximum density of precipitates during these three samples. In order to investigate the quality and quantity of the precipitates for these samples, the XRD patterns and the phase analysis results of precipitates are shown in Fig. 3 and Table 2. From Fig. 3, the peaks at $2\theta = 35°$, 40.8°, 49°, and 71° from TiC [15–17] (111), (200), (220), and (311), respectively, can be found in the XRD patterns (Fig. 3) for the samples A–C, which imply that the main precipitates of these samples are the TiC phase. It is interesting that other peaks also appear in addition to the peak from TiC. The peaks at $2\theta = 48.5°$, 53°, and 58° can be ascribed to Fe_3C (220), (202), and (231), respectively, which imply that the Fe_3C only found in as-quenched sample A, rather than the sample B and C. Table 2 shows that the precipitation content of Ti in sample A–C is 0.092, 0.14, and 0.16%, respectively. It seems that different heat treatment process can make the Ti precipitate in different contents.

Figure 4 shows grains with misorientation angle not lower than 15° for the experimental steels with different microstructures. According to the distributions of grain

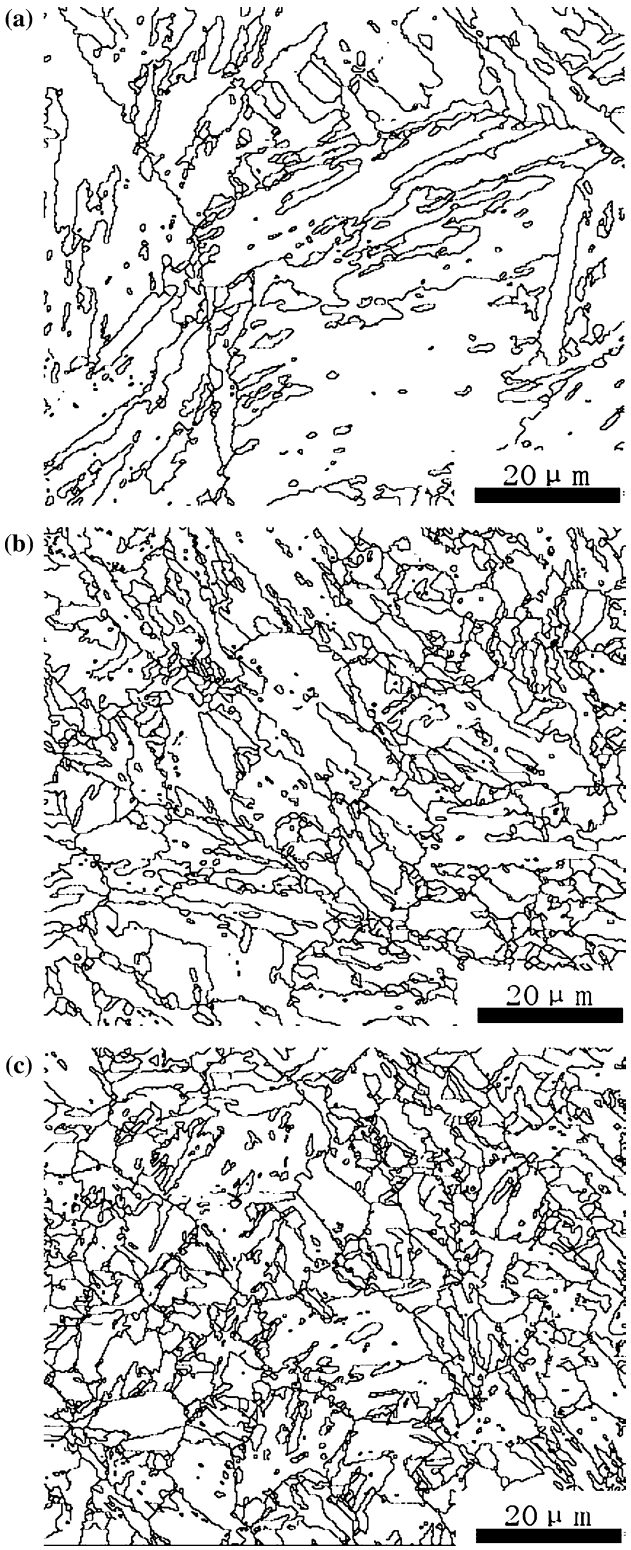

Fig. 4 EBSD orientation maps for **a** sample A, **b** sample B, and **c** sample C

boundary misorientation, the fractions of high-angle grain boundaries (HAGBs) with misorientation angles more than 15° for the samples A–C were estimated to be 60, 72 and 80%, respectively. It had been shown that after different heat treatments, the variations in fraction of HAGBs were achieved.

Figure 5 shows the size distribution of precipitates and precipitation content of Ti in precipitates for the samples A–C. From this figure, it can be seen that the mass fraction of TiC precipitates in diameter from 30 to 100 nm does not change too much during these three samples. However, the mass fraction of TiC precipitates in diameter from 1 to 10 nm changes significantly under different heat treatments. The sample A has the lowest mass fraction of fine TiC precipitates in diameter from 1 to 10 nm. In contrast, sample C has the highest mass fraction of TiC precipitates in diameter from 1 to 10 nm during those three samples. From Fig. 5, the difference of precipitation Ti between sample B and C is ~0.02%, which belongs to the 1–10 nano-sized TiC precipitates. In Table 2, the difference of precipitation Ti between sample B and C is ~0.02%. The only different heat treatment in sample B and C is the tempering process, in which sample C undergoing the tempering process between as-quenched and reheat quenching process. Therefore, we can conclude that the tempering process makes the ~0.02% Ti precipitate in the size of 1–10 nm. It is interesting that the mass fraction of relative bulky size TiC precipitates in diameter with 140–300 nm decreases in sample B and C after reheat quenching process compared with sample A. From the previously given results, it is not difficult to understand that the size distribution of TiC precipitates can be significantly influenced by the heat treatment. A large number of freshly nano-sized (1–10 nm) TiC precipitates are formed only in the reheat quenching sample C, rather than as-quenched sample A.

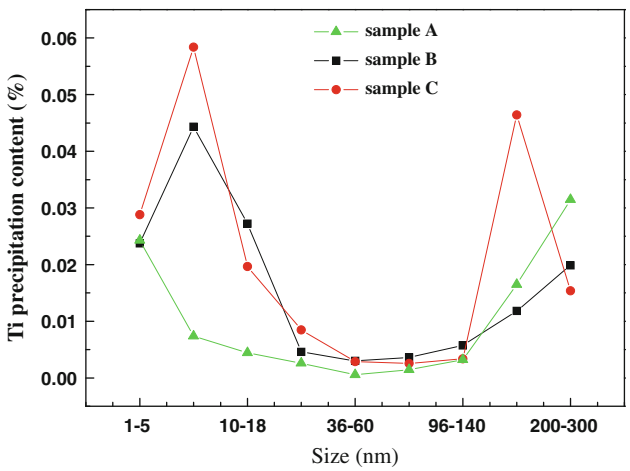

Fig. 5 The size distribution of precipitates and precipitation content of Ti in precipitates for sample A–C

Table 3 shows the mechanical properties from as-quenched sample A, reheat quenching sample B, and tempering–reheat quenching sample C, respectively, in which the yield strength from the measured samples is 1220, 1255, and 1280 Mpa. This means that the reheat quenching sample B has a better yield strength than that of as-quenched sample A, and the sample C has the best yield strength among three samples. It seems that the reheat quenching process is favorable to improve the yield strength for martensitic steel, and the yield strength of Ti-containing martensitic steel can be further enhanced by tempering and reheat quenching treatment. From the above results, it can be inferred that the tempering process plays an important role in the yield strength of martensitic steel in our case. Meanwhile, the total elongation and reduction in area also did not show any significant variation with change in yield strength in the present martensitic steel. It should be noted that the impact toughness also has been improved along with yield strength for the heat-treated sample B and C as compared to as-quenched sample A.

Comparing reheat quenching sample B with as-quenched sample A, the yield strength has been enhanced by reheat quenching process. As we know, the microstructure of the steel after quenching treatment was martensite, and, thus, martensitic hardenability is not considered to be a factor in these strength differences between the two samples. The average grain size is also an important factor to influence the yield strength of martensitic steel. Table 4 shows that there is significant difference in the average grain size between as-quenched A and reheat quenching sample B. The average grain size of sample B is about 10 μm (Fig. 4b), which is relative smaller than that of sample A with ~43 μm (Fig. 4a). It is well known that the grain refinement can enhance yield strength of the steel. The smaller the average grain size is, the better the yield strength is. Therefore, one reason of the yield strength enhancement for the sample B in the present case is grain

Table 3 The mechanical properties of samples

Sample	A	B	C
Yield strength (MPa)	1220	1255	1280
Total elongation (%)	12	14	13
Impact energy (J), −40 °C	10	24	32

Table 4 The grain size and ratio of HAGBs for the samples A–C

Sample	A	B	C
Grain size (μm)	43	10	8
High-angle grain boundaries (%)	60	72	80

refinement, which is mainly attributed to the TiC precipitates pinning austenitic grain boundaries during the reheat quenching process, favoring for reducing grain size. According to the conventional Hall–Petch equation [18]:

$$\sigma_y = Kd^{-1/2} + \sigma_0, \quad (1)$$

the value of contribution of grain refinement can be estimated as 70 Mpa, which may imply that the grain refinement after reheat quenching is a reason for the yield strength enhancement for the sample B. Concerning precipitates in this steel, most of the TiC precipitates present in the as-quenched steel should dissolve during the 1250 °C treatment before hot rolling. As a result, Ti is available for precipitation during subsequent process. Because the plates were finish rolled below about 850 °C, it is hypothesized that TiC precipitates formed on the deformation substructure of the austenite, thereby inhibiting austenite recrystallization. For the sample A, the steel plate was immediately quenched after hot rolling. As a result of quenching, it is expected that the titanium-containing substructure precipitates remain relatively fine. In addition, a significant portion of titanium remains in solid solution. Subsequent tempering at 550 °C would result in freshly formed TiC precipitates, finer than the substructure precipitates discussed above. During reheat quenching process, the relative bulky precipitates dissolved again and freshly formed fine TiC precipitates appear on the order of 1–10 nm in diameter, which may play an important role in the yield strength enhancement. It is well known that the yield strength of steels contain a contribution from the precipitation hardening, which is also described quantitatively by the Ashby–Orowan equation. According to Ashby–Orowan relationship [19]

$$\sigma_p = \left(0.538Gbf^{1/2}/X\right)\ln(X/2b) \quad (2)$$

where σ_p is the increase in yield strength (MPa), G is the shear modulus (MPa), b is the Burgers vector (mm), f is the volume fraction of particles, and X is the real (spatial) diameter of the precipitates (mm). According to Eq. 2, substituting the value of the mass fraction and size distribution of TiC precipitates in Fig. 5, the contribution from the precipitation hardening of samples A and B can be evaluated as 134 and 154 Mpa, respectively. However, this precipitation hardening is counteracted by an unexpected softening mechanism, which is attributed to the formation of TiC precipitates making the content of carbon in martensitic matrix decrease. Phase analysis results show that the difference in precipitation content of carbon between sample A and B is 0.012% (Table 2), which can bring the strength decrease with ~50 Mpa in martensitic matrix [20]. Then, the difference between precipitation hardening and grain refinement from TiC precipitates and decrease solid solution from carbon is the actual yield strength enhancement ~40 Mpa for the sample B.

The yield strength of tempering–reheat quenching sample C, compared to reheat quenching sample B, has been further improved. One possible reason may be attributed to the different average grain sizes. Table 4 shows that there is no appreciable difference in the average grain size between sample B and C. Therefore, the yield strength enhancement effect induced by average grain size can be negligible in the present case. Table 2 shows that there is ~0.02% Ti difference in the precipitates in the diameter of 1–10 nm between sample B and C, which may cause precipitation hardening difference in the martensitic steel. An important precipitation difference for the sample C is the presence of tempering stage of thermomechanical processing as compared to sample B. According to Eq. 2, the contribution from the precipitation hardening of sample C can be evaluated as 188 Mpa, which is higher ~30 Mpa than that of sample B. However, there is no significant change in the C precipitation between sample B and C. Then, the difference in the precipitation hardening from TiC is the actual yield strength enhancement ~30 Mpa for the sample C, which agrees well with the experimental results. Therefore, the yield strength enhancement of sample C in the present case can be mainly attributed to precipitation hardening increase after the introduction of tempering process.

The impact toughness of sample B, comparing with sample A, has been greatly improved after reheat quenching process. Table 4 and Fig. 4 show that there is significant difference in the average grain size between as-quenched sample A (Fig. 4a) and reheat quenching sample B (Fig. 4b). It is well known that the grain refinement can enhance the impact toughness of the steel. The smaller the average grain size is, the better the impact toughness is. Therefore, the improvement of impact toughness of sample B in the present case can be mainly attributed to grain refinement after the introduction of reheat quenching process. As for the sample C, the impact toughness has been further improved. One possible reason may be attributed to the different average grain size. Table 4 and Fig. 4 show that there is no appreciable difference in the average grain size between samples B (Fig. 4b) and C (Fig. 4c). Therefore, the impact toughness enhancement induced by average grain size can be negligible in the present case. Despite these similarities, they exhibited variation in toughness. The EBSD results shown in Table 4 indicate that the sample C has the highest HAGBs among these three samples. It was observed that steels with high toughness contained a very high fraction of HAGBs, where as low-toughness steel generally consisted of low fraction of HAGBs. These observations were consistent with the impact toughness data confirming that the

grain boundaries differences must have contributed to the observed variation in toughness of the examined steels. HAGBs were considered to change the cleavage crack propagation direction [21, 22], causing more difficult for crack propagation and behaving better toughness. The fraction of HAGBs in sample is the highest, followed by sample B and A. Therefore, the impact toughness (below −40 °C) of sample C is the best, then sample B and A, as shown in Table 3, well consistent with the comparison of fraction of HAGBs. Therefore, the variation of impact toughness between sample B and C can be mainly attributed to the difference of HAGBs after different heat treatments.

Conclusions

The effect of Ti addition on the yield strength and impact toughness for martensitic steel fabricated by vacuum induction melting has been investigated. It is found that the yield strength properties of martensitic steel can be improved by Ti addition, which is associated with precipitation hardening from formation of TiC precipitates in the martensitic matrix. Furthermore, it is found that the tempering and reheat quenching treatment can promote a formation of freshly nano-sized TiC in diameter from 1 to 10 nm and refine the average grain size to a superfine sized (∼8 μm) grains and lead to a further increase in the yield strength for martensitic steel-containing Ti, and the theoretical calculations are used to explain the yield strength enhancement. The results show that the formation of nano-sized precipitates after reheat quenching process act as obstacles to dislocation movement, which can result in precipitation hardening of 188 Mpa. EBSD results show that the martensitic steel treated by tempering and reheat quenching process has the highest ratio of HAGBs, which is the main reason why the impact toughness for martensitic steel is enhanced via titanium addition. This investigation sheds a deep light on the precipitation hardening and grain refinement for martensitic steel-containing Ti under different heat treatments.

Acknowledgement This research is supported by National Basic Research Program of China (973 program) No. 2010CB630803 and National High-tech R&D Programs (863 programs) No. 2511 and No. 2009AA033401.

References

1. Abd-Allah NM, El-Fadaly MS, Megahed MM, Eleiche AM (2001) J Mater Eng Perform 10:576
2. Ezugwu EO, Olajire KA (2002) Tribol Lett 12:183
3. Yilmaz R, Türkyilmazoglu A (2007) Adv Mater Res 23:319
4. Bhavsar RB, Montani E (1998) Corrosion 98:22
5. Oliver DA, Harris GT (1952) Iron Steel Inst 43:46
6. Davies WT, Hall B (1967) Iron Steel Inst 97:561
7. Angeliu T, Hall EL, Larsen M, Linsebigler A, Mukira C (1999) Inst Mater 708:234
8. Parameswaran P, Vijayalakshmi M, Shankar P, Raghunathan VS (1992) J Mater Sci 27:5426. doi:10.1007/BF00367811
9. Martin R, Mari D, Schaller R (2009) Mater Sci Eng A 521–522:117
10. Song YY, Ping DH, Yin FX, Li XY, Li YY (2010) Mater Sci Eng A 527:614
11. Bhambri SK (1986) J Mater Sci 21:1741. doi:10.1007/BF01114734
12. Ikeda S, Sakai T, Fine ME (1977) J Mater Sci 12:675. doi:10.1007/BF00548157
13. Barani AA, Li F, Romano P, Ponge D, Raabe D (2007) Mater Sci Eng A 463:138
14. Yaggee FL, Gilbert ER, Styles JW (1969) J Less Common Met 19:39
15. Baviera P, Harel S, Garem H, Grosbras M (2001) Scr Mater 44:2721
16. Mani A, Aubert P, Mercier F, Khodja H, Berthier C, Houdy P (2005) Surf Coat Technol 194:190
17. Li SB, Xiang WH, Zhai HX, Zhou Y (2008) Powder Technol 185:49
18. Friedman LH, Chrzan DC (1998) Phys Rev Lett 83:2715
19. Cao JC, Yong QL, Liu QY, Sun XJ (2007) J Mater Sci 42:10080. doi:10.1007/s10853-007-2000-4
20. Sagaradze VS (1970) Met Sci Heat Treat 12:198
21. Diaz-Fuentes M, Iza-Mendia A, Gutierrez I (2003) Metall Mater Trans 34A:2505
22. Wang BH, Kim YG, Lee S, Kim YM, Kim NJ, Yoo JY (2005) Metall Mater Trans 36A:2107